(Received 25 March 2024, Accepted 27 April 2024, Scheduled 12 May 2024)

Cross Polar Reduction of a High Gain Wide-Band Stacked Microstrip Antenna Using Metasurfaces

Anjali Rochkari[1], Shubhangi Verulkar[2], Nayana Chaskar[3], Mahadu Trimukhe[1], and Rajiv Gupta [1,*]

[1]*Department of Electronics and Telecommunication, Terna Engineering College, Nerul, Navi-Mumbai, India*
[2]*K. C. College of Engineering and Management Studies and Research, Thane, Mumbai, India*
[3]*M.H. Saboo Siddik College of Engineering, Byculla, Mumbai, India*

ABSTRACT: In this article, a low-profile high gain stack microstrip antenna (MSA) with low Cross Polarization Level (CPL) using multiple meta-surfaces is proposed. MSA on a thick substrate having low dielectric constant enhances the gain and bandwidth (BW). However, as substrate thickness increases, the CPL increases due to the increase in coaxial probe length used for feeding MSA. The CPL is reduced by using metasurfaces formed by an array of square metallic patches of dimensions and periodicity $< 0.1\lambda_0$. A suspended MSA (SMSA) is designed on a reactive impedance surface (RIS) backed substrate, to reduce the interaction between substrate and ground plane, surface waves and to increase impedance BW and polarization purity. A parasitic patch is fabricated on a superstrate and placed above the SMSA and metallic patches forming the metasurfaces are fabricated around the MSA, parasitic patch (PP) and on the other side of superstrate. These metasurfaces increase the inductance of the antenna, and to compensate the inductance, the height of SMSA and the spacing between MSA and PP are decreased which results in the decrease in probe feed length and CPL. This novel low-profile high gain wide band stack MSA offers CPL < -20 dB, Side Lobe Level (SLL) < -20 dB, Front to Back lobe ratio (F/B) > 20 dB, and $S_{11} \leq -10$ dB over 3.3–3.6 GHz to cover 5G applications. The $0.935\lambda_0 \times 0.99\lambda_0 \times 0.046\lambda_0$ prototype antenna offers peak gain of 8.3 dBi, antenna efficiency $> 90\%$, and λ_0 being the free-space wavelength at 3.3 GHz.

1. INTRODUCTION

There are applications such as 5G and 6G where high gain with large BW is of prime importance for the merits of high transmission rate, high capacity, and low power consumption. 5G and 6G technologies offer seamless connectivity. Reliable access with high data rate and low latency has made virtual business using augmented reality a part of our life. Significant bearing on the economy has motivated researchers to improve performance and functionality of 5G technology and deploy 5G networks. It has provided an impetus to the design of novel antennas for 5G applications.

MSA has limitations of narrow impedance BW, low gain, and low efficiency. The gain and BW of MSA can be increased by decreasing effective dielectric constant and thickness of the substrate. However, the size of antenna increases with the decrease in dielectric constant. Further, the substrate height cannot be increased beyond a limit as the impedance becomes inductive with the increase in height of substrate, and beyond certain height MSA cannot be matched [1]. Further, radiation due to probe feed length increases the CPL with the increase in substrate height.

BW can also be increased by using multi-resonator concept. MSA and parasitic patches in planar or stack configuration offer broad BW. However, this increases the dimensions of antenna, and radiation pattern varies over the band. Reactive impedance surface (RIS), metasurface (MS), electromagnetic band gap (EBG), high impedance surface (HIS), and artificial magnetic conductors (AMCs) are widely used to improve the performance of antennas [2–4]. RIS, metasurface, HIS, EBG, and AMC are generally designed by using periodic geometries having dimensions and periodicity smaller than wavelength [2–4]. Fabry Perot cavity resonators have been reported which offer high gain and wide BW but suffer from high profile, large dimensions, high SLL and CPL [5–9].

Low profile antenna arrays using RIS and PRS have been reported [10, 11]. A high gain low profile antenna using a non-zero index (NZI) MS lens is designed with improved front to back ratio (FBR) [12]. Nonuniform RIS with parasitic strips is used to improve the performance of Circularly Polarized (CP) antenna [13].

The gain and BW of antenna can be enhanced by using stack patches above MSA [14–16]. A broadband high gain multi-layer antenna is designed by placing two circular patches above a metallic circular or elliptical MSA [14]. 12.1 dBi peak gain with 55.7% BW is obtained. However, the antenna has high SLL and CPL. A double cavity backed multi-resonator stack antenna is designed to provide 12.5 dBi average gain. The antenna has low CPL, but high SLL located away from half-power beamwidth [15]. A broadband high gain stack antenna using triangular patches is designed. The antenna offers 10.8 dBi peak gain but -13.6 dB SLL and 15.8 dB FBR [16]. An anisotropic elliptical metasurface is used to enhance the axial ratio BW of a CP antenna [17]. The antenna offers 8.6 dBi gain with -14 dB SLL.

* Corresponding author: Rajiv Gupta (rajivgupta@ternaengg.ac.in).

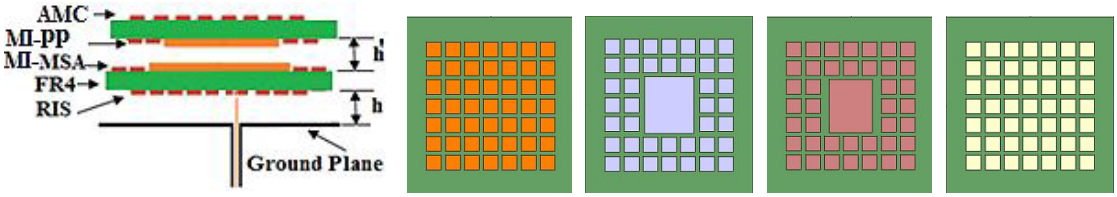

FIGURE 1. Side view of proposed antenna along with top view of RIS, MI-MSA, MI-PP and AMC.

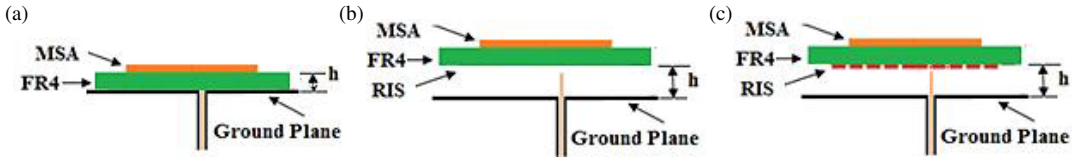

FIGURE 2. Side view of (a) MSA, (b) SMSA, (c) SMSA-RIS.

Thus, a novel low-profile stacked suspended MSA is designed using multiple metasurfaces. These RIS/AMC surfaces not only increase the BW and gain of antenna but also reduce CPL and SLL. The compact antenna is designed to cover 3.3–3.6 GHz, 5G band with SLL and CPL < 20 dB and F/B lobe ratio > 20 dB. The antenna is easy to feed and fabricate, small, and in low cost.

2. ANTENNA GEOMETRY AND DESIGN THEORY

The side view of the proposed antenna along with the top view of four metasurface layers is shown in Fig. 1. (i) The first metasurface RIS, formed by an array of 7 mm side length of small square metallic patches with periodicity of 9 mm is printed on the bottom side of 1.59 mm thick FR4 dielectric substrate-1 and placed 1 mm above the 0.5 mm metal ground plane. (ii) The second metasurface formed by an array of 7 mm side length of small square metallic patches is printed on the top side of 1.59 mm thick FR4 dielectric substrate-1 around MSA, called metamaterial inspired MSA layer (MI-MSA). (iii) The third metasurface formed by an array of 7 mm side length of small square metallic patches is printed on the bottom side of 1.59 mm thick FR4 dielectric substrate-2 around a rectangular parasitic patch (PP), called metamaterial inspired PP layer (MI-PP). (iv) The fourth metasurface AMC formed by an array of 7 mm side length of small square metallic patches is printed on the top side of 1.59 mm thick FR4 dielectric substrate-2 and placed 1.5 mm above the dielectric substrate-1, termed as AMC. The distance between ground plane and dielectric substrate-1 is 1 mm, and the distance between dielectric substrate-1 and dielectric substrate-2 is 1 mm. The dielectric constant and loss tangent of 1.59 mm thick dielectric substrate-1 and dielectric substrate-2 are 4.4 and 0.02, respectively. The suspended MSA is fed through a coaxial probe of 50 Ω. The design theory and step-by-step evolution of the proposed structure are described below.

Bandwidth and gain of suspended MSA increase due to the increase in substrate height and decrease in effective dielectric constant. However, as the substrate height increases, the probe inductance and probe length play a significant role. The impedance matching becomes difficult due to inductive probe reactance beyond a certain substrate height, and the probe acts as a monopole antenna leading to cross polarization [1].

RIS consisting of an array of square patches of dimensions and periodicity $< 0.1\lambda_0$ reduces the interaction between MSA and ground plane, improves impedance matching, reduces surface waves, and thus improves polarization purity [2, 3, 10, 11, 18]. An array of square patches of dimensions and periodicity $< 0.1\lambda_0$ forms AMC and increases inductance of the structure, and to compensate this inductive effect substrate height is decreased which increases the capacitance formed between patch and ground plane. It results in the decrease in probe inductance and also CPL due to the decrease in probe length [10, 11].

The PP above the suspended MSA (SMSA) results in a multi-resonator structure. When the SMSA and PP resonate at two different but nearby frequencies, they electromagnetically couple to result in wide impedance BW. The bandwidth depends on coupling factor, MSA and PP patch dimensions, and the spacing between them. The tight coupling results in small BW but poor coupling result in dual bands or narrow BW. However, coupling should be optimized to obtain large BW [1]. In the proposed antenna, PP and MSA are tightly coupled, and the surface current on PP increases the inductance of the structure, and therefore, to compensate the inductive effect, capacitance is increased by decreasing the substrate height. The decrease in substrate height results in the decrease in probe length and radiation due to it. It results in the decrease in CPL.

Initially, a rectangular MSA of 19.8 mm $\times$ 24.3 mm is designed on a 1.59 mm thick FR4 substrate as shown in Fig. 2(a). The dielectric constant of the FR4 substrate is 4.4, and its loss tangent is 0.02. The ground plane dimensions are 50 mm $\times$ 55 mm. The antenna offers the peak gain of 4.0 dBi and $S_{11} \leq -10$ dB over 3.4–3.51 GHz. The dimensions of antenna are calculated using standard equations [1]. The structures are simulated using IE3D 15.0 version software.

To enhance the BW and gain of antenna, a suspended MSA (SMSA) on an FR4 substrate as shown in Fig. 2(b) is designed. A rectangular MSA of 30 mm $\times$ 35 mm is designed on an FR4

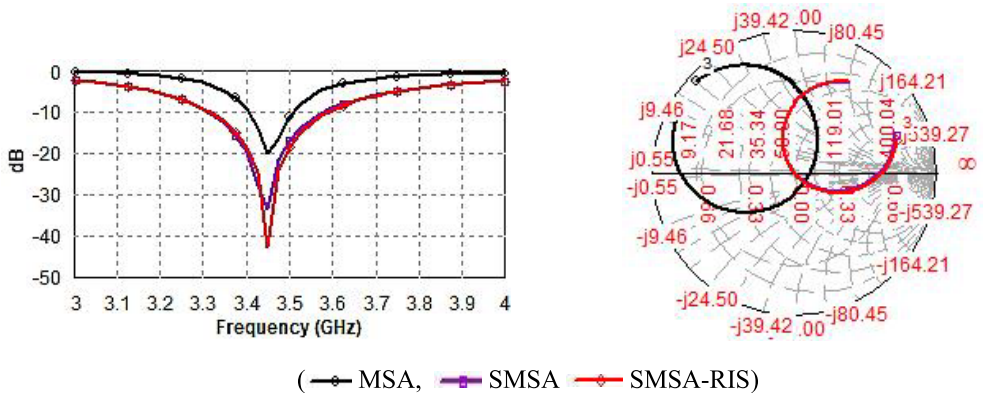

FIGURE 3. S_{11} and impedance variation.

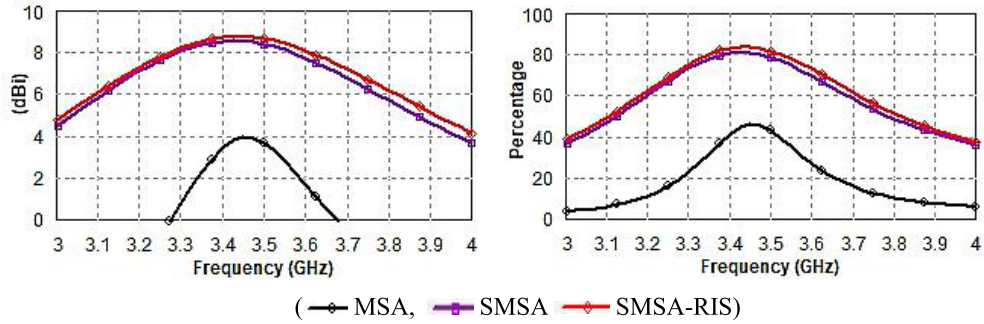

FIGURE 4. Gain and antenna efficiency.

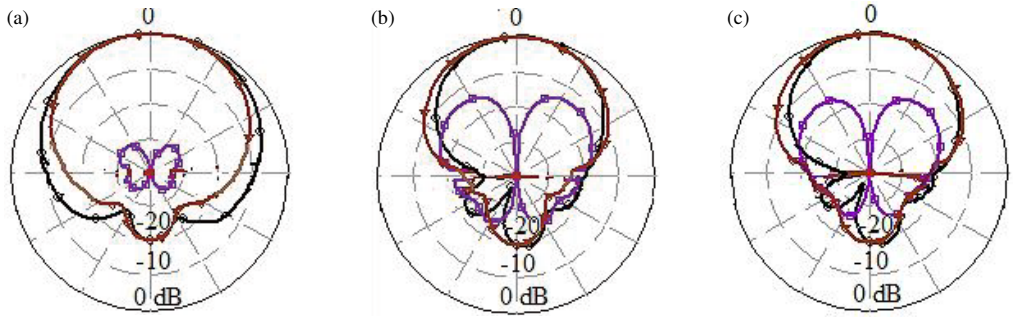

FIGURE 5. Radiation pattern at 3.45 GHz. (a) MSA, (b) SMSA, (c) SMSA-RIS.

substrate and suspended in air at 3.5 mm from 80 mm × 85 mm ground plane. SMSA offers the peak gain of 8.1 dBi and $S_{11} \leq -10$ dB over 3.3–3.6 GHz for 5G applications. S_{11} and impedance variation plots of MSA and SMSA are shown in Fig. 3.

The SMSA is then designed on a reactive impedance surface (RIS) backed FR4 substrate as shown in Fig. 2(c). RIS consists of an array of metallic patches having dimension and periodicity $< 0.1\lambda_0$ [18]. The RIS layer, 7 × 7 array of 7 mm square patches with uniform center to center spacing of 9 mm, is fabricated on the other side of the FR4 substrate. It is suspended in the air at a height of about 3.0 mm from the ground plane. The antenna is termed as SMSA-RIS. The conducting square patches of 7 × 7 array of RIS are equivalent to inductance, and the gap between the square patches is equivalent to capacitance. Therefore, the reactive impedance of the structure increases. As a result, the resonant frequency of SMSA decreases when it is designed on an RIS backed substrate. Therefore, the substrate height is decreased to 3.0 mm, and the dimensions of SMSA are decreased to 27 mm × 29.6 mm so that the structure resonates at 3.45 GHz. RIS reduces the interaction between the substrate and ground plane and thus reduces the surface waves and increases the efficiency of the antenna. It also helps in improving impedance BW and CPL. The gain and antenna efficiency of MSA, SMSA, and SMSA-RIS are shown in Fig. 4.

The radiation patterns of MSA, SMSA, and SMSA-RIS are shown in Fig. 5. MSA offers low gain and wide beamwidth. The ground plane dimensions are optimized so that the front

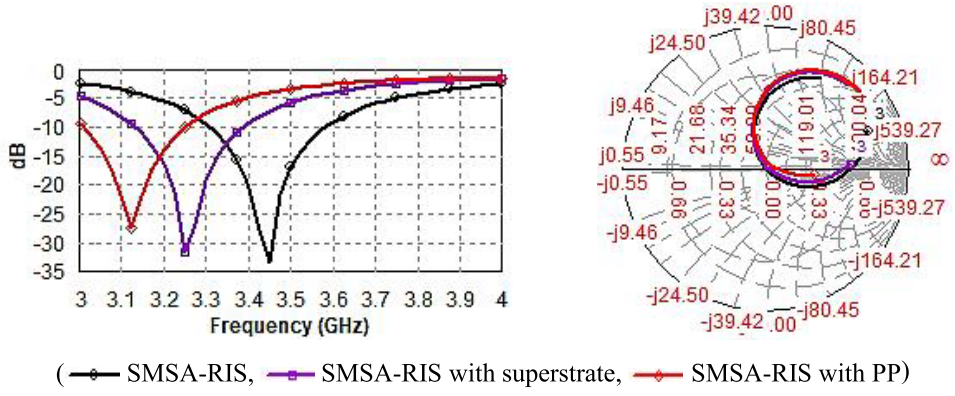

FIGURE 6. S_{11} and impedance variation.

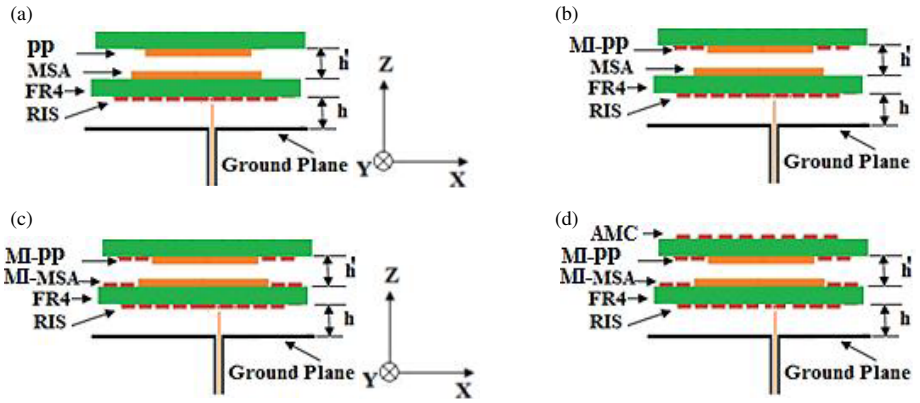

FIGURE 7. Geometry of different configuration of stack SMSA. (a) ST-MSA-RIS. (b) MI-ST-MSA-RIS. (c) MI-ST-MI-MSA-RIS. (d) AMC-MI-ST-MI-MSA-RIS.

to back lobe ratio is about 20 dB. SMSA offers higher gain and BW but has high CPL < -14 dB. In SMSA, the CPL increases with the increase in substrate height due to radiation from probe feed whose length increases with the increase in substrate height. The CPL in SMSA-RIS is < -15.5 dB. CPL improves in SMSA-RIS as RIS helps in increasing the field in the same direction in which MSA radiates. Further, substrate height is decreased to 3.0 mm in SMSA-RIS to operate it over 3.3–3.6 GHz. SMSA-RIS also offers higher gain and antenna efficiency than SMSA despite about 10% less dimensions than the SMSA. SMSA-RIS offers 8.2 dBi peak gain.

3. STACKED SUSPENDED MSA ON RIS BACKED SUBSTRATE

The SMSA on the RIS backed FR4 substrate is designed in Section 2. A rectangular patch is fabricated on one side of the FR4 substrate while the RIS layer, 7×7 array of 7 mm square patches with uniform center to center spacing of 9 mm, is fabricated on the other side of FR4. It is suspended in the air at a height of 3 mm from the ground plane. Now a 1.59 mm thick FR4 superstrate is placed at a height 1 mm above the MSA. Superstrate increases the effective dielectric constant, and therefore resonating frequency of the structure decreases as shown in Fig. 6. Now a 26.5 mm $\times$ 29.1 mm parasitic patch (PP) is fabricated on one side of FR4 superstrate facing the MSA as shown in Fig. 7(a). The resonating frequency of the structure further decreases. The PP electromagnetically couples with MSA. The resonant frequency of the structure depends on the dimensions of PP and the spacing between PP and the MSA [1]. S_{11} and impedance variation of SMSA-RIS, SMSA-RIS with superstrate, and SMSA-RIS with PP are shown in Fig. 6.

The substrate height is decreased to 2.5 mm to increase the resonating frequency and to improve CPL. The structure is optimized. The dimensions of rectangular MSA and parasitic patch are 25.8 mm $\times$ 29.2 mm and 22 mm $\times$ 26 mm, and the parasitic patch is placed at 2 mm from MSA. $S_{11} < -10$ dB is obtained over 3.3–3.6 GHz. Stacked MSA on RIS backed substrate (ST-MSA-RIS), shown in Fig. 7(a), offers 8.6 dBi peak gain. The F/B is about 20 dB and CPL < -16 dB.

An array of 7 mm square patches with uniform center to center spacing of 9 mm is fabricated all around the PP on the same side of FR4 superstrate to form a metamaterial inspired stack MSA (MI-ST-MSA-RIS) as shown in Fig. 7(b). It increases the inductive impedance of the structure and thus decreases the resonant frequency. The substrate height is further decreased, and the dimensions of MSA, PP patch, and the spacing between the MSA and PP are optimized so that the structure operates over 3.3–3.6 GHz. The substrate height is decreased to 1.5 mm, and the distance between MSA and PP is decreased to 1.7 mm.

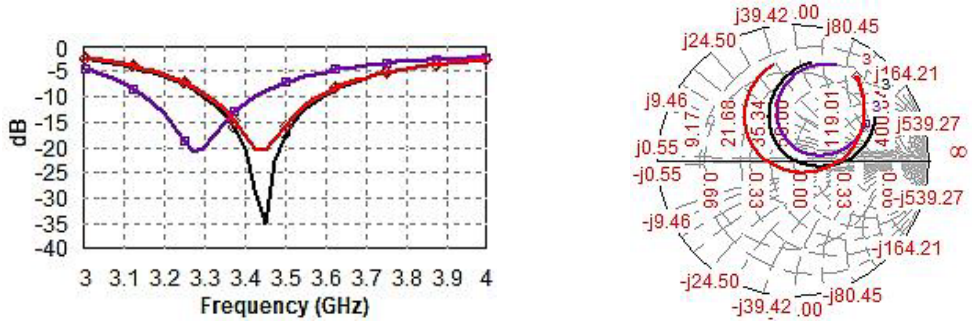

FIGURE 8. S_{11} and impedance variation.

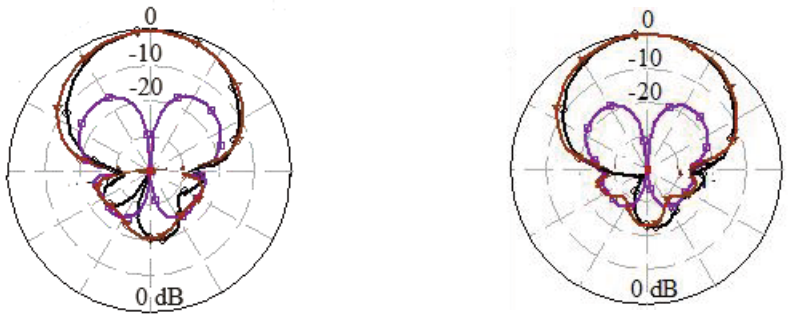

FIGURE 9. Radiation pattern at 3.45 GHz.

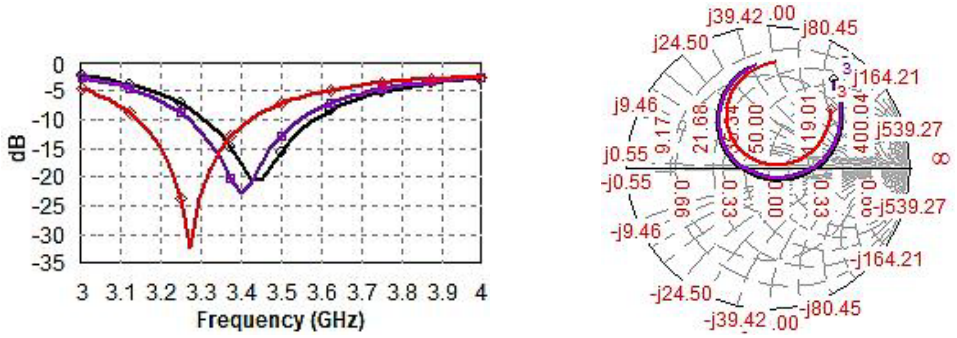

FIGURE 10. S_{11} and impedance variation.

The dimensions of MSA and PP are 25.2 mm × 29 mm and 21 mm × 26 mm, respectively. S_{11} and impedance variation of ST-MSA-RIS, MI-ST-MSA-RIS, and optimized MI-ST-MSA-RIS are shown in Fig. 8. $S_{11} < -10$ dB is obtained over 3.3–3.6 GHz. The optimized MI-ST-MSA-RIS offers 8.6 dBi peak gain. The F/B is about 20 dB and CPL < -18 dB as shown in Fig. 9.

Now, an array of 7 mm square patches, with uniform center to center spacing of 9 mm, is placed all around the MSA on the same side of FR4 superstrate to form a stack antenna consisting of metamaterial inspired PP and metamaterial inspired MSA (MI-ST-MI-MSA-RIS) fabricated on an RIS backed FR4 substrate, as shown in Fig. 7(c). It results in the decrease in resonant frequency due to the increase in the inductive impedance of the structure. Then, an array of 7 mm square patches, with uniform center to center spacing of 9 mm, is also fabricated on the other side of FR4 superstrate and termed as AMC-MI-ST-MI-MSA-RIS, as shown in Fig. 7(d). It further increases the inductive impedance of the structure and thus decreases the resonant frequency. S_{11} and impedance variation of these structures are shown in Fig. 10.

The dimensions of MSA are decreased in MI-ST-MI-MSA-RIS to obtain $S_{11} < -10$ dB over 3.3–3.6 GHz. The substrate height is decreased, and the dimensions of MSA, PP patch, and the spacing between the MSA and PP are optimized in AMC-MI-ST-MI-MSA-RIS so that the structure operates from

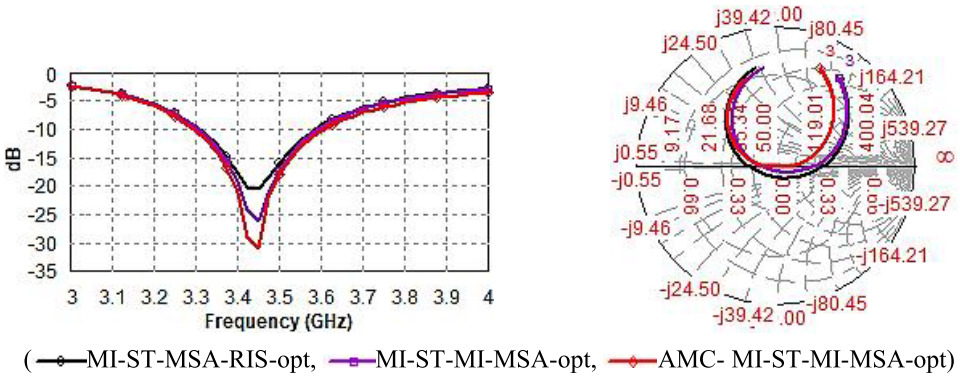

FIGURE 11. S_{11} and impedance variation.

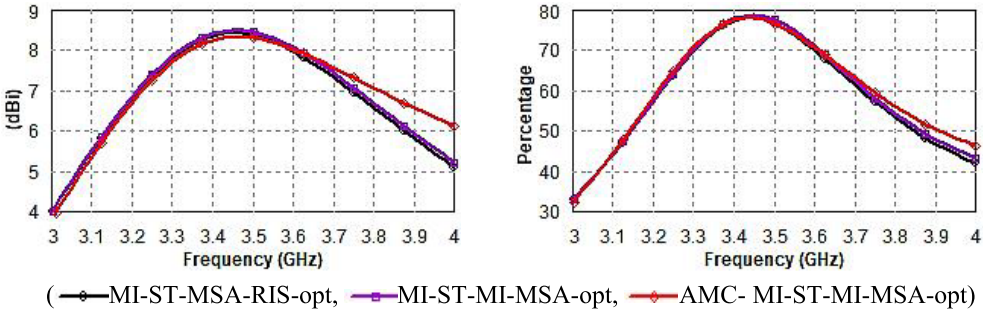

FIGURE 12. Gain and antenna efficiency.

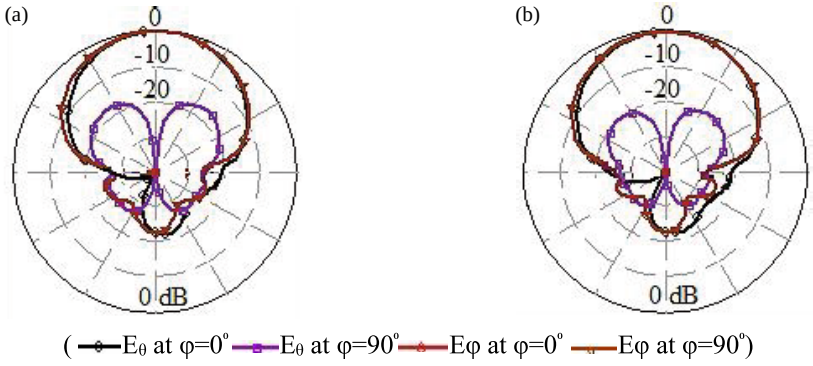

FIGURE 13. Radiation pattern at 3.45 GHz. (a) MI-ST-MI-MSA-RIS-opt. (b) AMC-MI-ST-MI-MSA-RIS-opt.

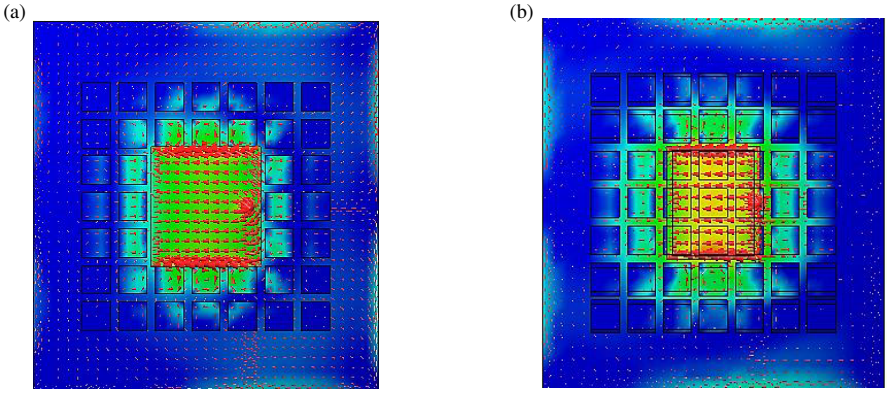

FIGURE 14. Surface current density. (a) SMSA-RIS. (b) AMC-MI-ST-MI-MSA-RIS-op.

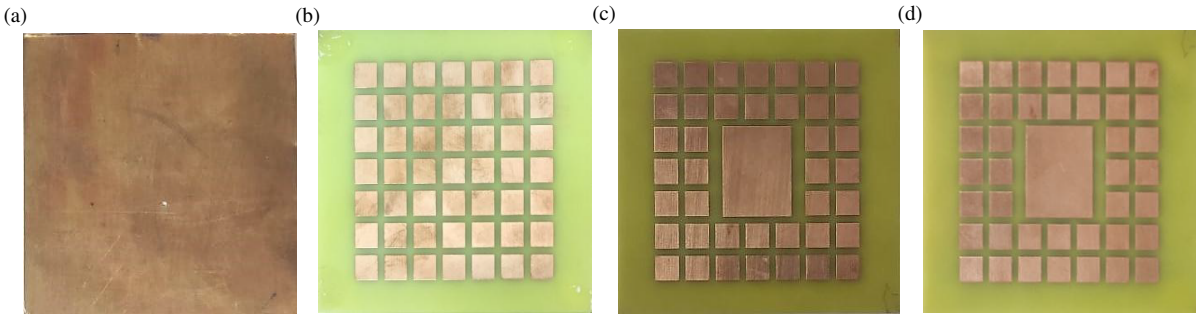

FIGURE 15. Top view of different layers of fabricated antenna. (a) Ground plane. (b) RIS/AMC. (c) MI-MSA. (d) MI-PP.

FIGURE 16. 3-dimensional view.

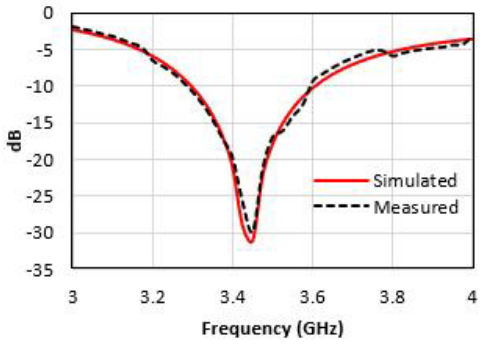

FIGURE 17. Simulated and measured S_{11}.

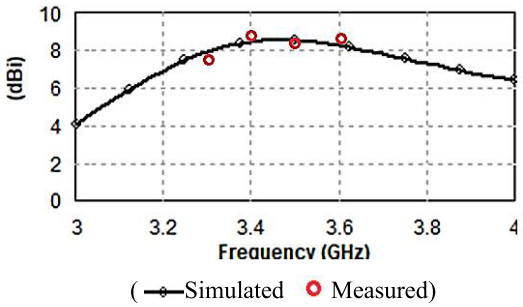

FIGURE 18. Simulated and measured gain.

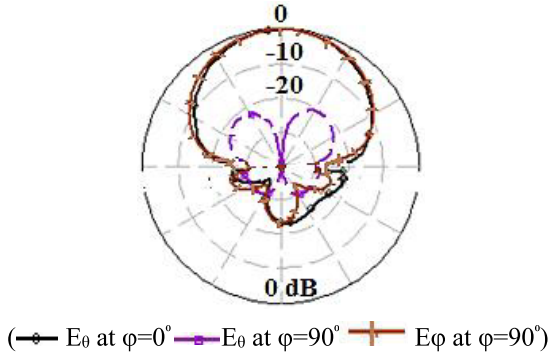

FIGURE 19. Measured radiation pattern 3.45 GHz.

3.3 to 3.6 GHz. The substrate height is decreased to 1.0 mm, and the distance between MSA and PP is optimized to 1.5 mm. The dimensions of MSA and PP are 23.4 mm × 27.2 mm and 20.4 mm × 25.4 mm, respectively. S_{11} and impedance variation of optimized MI-ST-MSA-opt, and MI-ST-MI-MSA-opt and AMC-MI-ST-MI-MSA are shown in Fig. 11. $S_{11} < -10$ dB is obtained over 3.3–3.6 GHz. The gain variation and antenna efficiency of the structures are shown in Fig. 12. The optimized MI-ST-MI-MSA offers 8.4 dBi peak gain. The F/B is about 20 dB and CPL < -17 dB whereas the optimized AMC-MI-ST-MI-MSA offers 8.3 dBi peak gain. The F/B is about 20 dB and CPL < -20 dB as shown in Fig. 13.

The reduction in CPL can also be explained by surface current density distribution. The scalar and vector surface current density distribution of suspended MSA on RIS backed substrate (SMSA-RIS) and proposed antenna 'AMC-MI-ST-MI-MSA-RIS-opt' are shown in Fig. 14. The significant surface current in orthogonal direction on MSA patch and ground plane in SMSA-RIS is responsible for higher CPL. There is negligible surface current in orthogonal direction on MSA patch and ground plane in proposed antenna. As a result, CPL decreases, and CPL < -20 dB is obtained in the proposed antenna.

4. FABRICATION AND MEASUREMENT RESULTS

The proposed antenna (PA) structure 'AMC-MI-ST-MI-MSA-RIS-opt' is fabricated. S_{11} and radiation pattern at 3.45 GHz are measured using Agilent Field fox N 9116A network analyzer and standard horn antenna in an anechoic chamber, respectively. The top view of each layer, 3-dimensional view of

antenna, and simulated and measured S_{11} are shown in Figs. 15, 16, and 17, respectively. The simulated and measured gain variation and measured radiation pattern at 3.45 GHz are shown in Figs. 18 and 19, respectively. The measured results closely align with simulated ones. The slight discrepancy in measured results from simulated results can be attributed to fabrication error, SMA connector loading, or misalignment of different layers in prototype antenna.

5. CONCLUSION

A low profile compact high gain stacked MSA with low CPL is designed using multiple metasurfaces. These metasurfaces increase the inductance of structure; therefore, the substrate height and spacing between MSA and PP are decreased to increase the capacitance to balance out the increase in inductance. It results in a decrease in probe feed length and CPL. The antenna operates over 3.3–3.6 GHz and offers 8.3 dBi peak gain with CPL and SLL < -20 dB, F/B lobe ratio > 20 dB, and antenna efficiency $> 90\%$. The structure is suitable for 5G applications. The antenna has additional advantages of simple design, small size, and low cost.

REFERENCES

[1] Kumar, G. and K. P. Ray, *Broadband Microstrip Antennas*, Artech House, Norwood, MA, 2002.

[2] Meng, F., Y. Liu, and S. K. Sharma, "A miniaturized patch antenna with enhanced bandwidth by using reactive impedance surface ground and coplanar parasitic patches," *International Journal of RF and Microwave Computer-Aided Engineering*, Vol. 30, No. 7, e22225, 2020.

[3] Guthi, S. and V. Damera, "High gain and wideband circularly polarized S-shaped patch antenna with reactive impedance surface and frequency-selective surface configuration for Wi-Fi and Wi-Max applications," *International Journal of RF and Microwave Computer-Aided Engineering*, Vol. 31, No. 11, e22865, 2021.

[4] Guthi, S. and V. Damera, "High gain and wide band antenna based on FSS and RIS configuration," *Radioengineering*, Vol. 30, No. 1, 96–103, 2021.

[5] Deng, F. and J. Qi, "Shrinking profile of Fabry-Perot cavity antennas with stratified metasurfaces: Accurate equivalent circuit design and broadband high-gain performance," *IEEE Antennas and Wireless Propagation Letters*, Vol. 19, No. 1, 208–212, 2020.

[6] Chaskar, N., S. D. Jagtap, R. Thakare, and R. K. Gupta, "Gain bandwidth enhancement of microstrip antenna fed half wavelength Fabry Perot cavity antenna," *International Journal of RF and Microwave Computer-Aided Engineering*, Vol. 31, No. 7, e22695, 2021.

[7] Chaskar, N., S. D. Jagtap, R. Thakare, and R. K. Gupta, "Gain flattening of wideband FPC antenna using elliptical and rectangular slotted AMC layers," *Progress In Electromagnetics Research C*, Vol. 110, 81–89, 2021.

[8] Singh, A. K., M. P. Abegaonkar, and S. K. Koul, "Wide gain enhanced band high gain Fabry-Perot cavity antenna using ultra-thin reflecting metasurface," *Microwave and Optical Technology Letters*, Vol. 61, No. 6, 1628–1633, 2019.

[9] Singh, A. K., M. P. Abegaonkar, and S. K. Koul, "High-gain and high-aperture-efficiency cavity resonator antenna using metamaterial superstrate," *IEEE Antennas and Wireless Propagation Letters*, Vol. 16, No. 6, 2388–2391, 2017.

[10] Jagtap, S., A. Chaudhari, N. Chaskar, S. Kharche, and R. K. Gupta, "A wideband microstrip array design using RIS and PRS layers," *IEEE Antennas and Wireless Propagation Letters*, Vol. 17, No. 3, 509–512, 2018.

[11] Rochkari, A., S. Verulkar, M. Trimukhe, V. Bodade, and R. Gupta, "Low profile high gain wideband stacked MSA array for 5G, WLAN and C-band applications," *International Journal of Microwave & Optical Technology*, Vol. 19, No. 1, 1–9, 2024.

[12] Singh, A. K., M. P. Abegaonkar, and S. K. Koul, "Compact near zero index metasurface lens with high aperture efficiency for antenna radiation characteristic enhancement," *IET Microwaves, Antennas & Propagation*, Vol. 13, No. 8, 1248–1254, 2019.

[13] Zheng, Q., C. Guo, J. Ding, and G. A. E. Vandenbosch, "Use of non-uniform RIS and parasitic strips to improve antenna CP performance," *IET Microwaves, Antennas & Propagation*, Vol. 14, No. 14, 1795–1802, 2020.

[14] Chopra, R. and G. Kumar, "Broadband and high gain multilayer multiresonator elliptical microstrip antenna," *IET Microwaves, Antennas & Propagation*, Vol. 14, No. 8, 821–829, 2020.

[15] Raha, K. and K. P. Ray, "Broadband high gain and low cross-polarization double cavity-backed stacked microstrip antenna," *IEEE Transactions on Antennas and Propagation*, Vol. 70, No. 7, 5902–5906, 2022.

[16] Chopra, R. and G. Kumar, "High gain broadband stacked triangular microstrip antennas," *Microwave and Optical Technology Letters*, Vol. 62, No. 9, 2881–2888, 2020.

[17] Srivastava, K., S. Kumar, S. Dwari, B. K. Kanaujia, H. C. Choi, and K. W. Kim, "Anisotropic meta-surface-based wideband high gain circularly polarized patch antenna," *Electromagnetics*, Vol. 40, No. 8, 594–604, 2020.

[18] Chaskar, N., S. Dalvi, S. Rathod, A. A. Chaudhari, and R. K. Gupta, "Effect of dimension, spacing, periodicity and shape of ris on resonant frequency and bandwidth of 2×2 antenna array," in *2016 Progress In Electromagnetic Research Symposium (PIERS)*, 4132–4136, Shanghai, China, Aug. 2016.